View metadata, citation and similar papers at core.ac.uk

brought to you by CORE

provided by NASA Technical Reports Server

REPORT NO. GDC-DBE-67-013

68N 10954

BASE FLOW FIELD INVESTIGATION ON THE S-II STAGE

By
L. D'Attorre and H. U. Thommen

March 1967

Submitted to
National Aeronautics and Space Administration
GEORGE C. MARSHALL SPACE FLIGHT CENTER
Huntsville, Alabama

Prepared under
Contract NAS8-21039

Prepared by
Space Sciences Laboratory
CONVAIR DIVISION OF GENERAL DYNAMICS
San Diego, California

Abstract

The calculation of the three dimensional interaction region of multi jet configurations by a finite difference method; the general description of the problem and the correspondent computer program have been given by the same authors in report GDC-DBE-66-014, May 1966.

In the present report, the computer program is re-examined in an attempt to reduce the number of parameters to be judged by the users. In conjunction a new finite difference method is introduced, which automatically provides an amount of dissipation appropriate to the requirements of the local flow conditions.

In order to test the effectiveness of the additional dissipation mechanism a number of experiments were performed. As a consequence of those studies a simplified program is obtained and when applied to the calculation of five jet interactions, yields result which are at least of equal quality of those previously reported.

Table of Contents

1. Introduction

Under contract NAS8-20101, a computer program was developed for the calculation of the inviscid interaction regions of multiple rocket engines (Ref. 1). The calculations were based on the finite difference method reported in Ref. 2.

Unfortunately, the results of these calculations suffered from the very adverse conditions to which they had to be applied. First, the interaction shocks are in general very little inclined to the plane of symmetry. Secondly, and more critical for the application of the finite difference method, the allowable step size Δx in marching direction was very small. This was caused by the relatively large velocity components normal to the marching direction. The effect of the small step size is that very strong oscillations are observed in the tail end of shock waves which are poorly damped. Such results are very difficult to interpret.

In Ref. 1, a variety of methods were investigated by which these oscillations could be damped.

The problem has now been reinvestigated and the results are presented in this report.

For convenient reference, the basic differential equations are repeated in Section 2. A new difference scheme is described in Section 3, and an additional damping mechanism is introduced.

The effectiveness of the damping procedure is investigated in Sections 4 and 5. Although the principal mechanism is the same, for practical application there are two different approaches possible. A number of simple experiments were performed using a single value of the damping parameter

in each plane. The results are presented in Section 4. It was found that this damping parameter was strongly dependent on the gas dynamic properties. Although a relatively simple correlation was obtained between the most favorable damping factor and the pressure ratio across the shock, application of this correlation law to the much more complicated case of multiple jet interaction seems very difficult. Therefore, a second damping procedure is introduced in Section 5. This method has the advantage that it is only indirectly related to the gas dynamic conditions. It makes use of the local properties, i.e., the damping parameter is chosen according to the local conditions. It requires choice of one single parameter, ϵ, and the tests carried out so far indicate that the value of this parameter can be chosen a priori as about 0.5 to 0.75.

This method of damping was incorporated into the program described in Ref. 1, and all the previously used methods have been deleted. This simplified program has been found to yield results which are at least of equal quality to those reported in Ref. 1. On the other hand, this program does not require any judgment by the operator above the choice of the single parameter ϵ. The results of a test calculation for the five-jet interaction is presented in Section 6. The results show a behavior quite similar to that obtained by the method of characteristics in Ref. 3, although in this paper a much simpler problem was investigated.

2. The Differential Equation

We consider a cartesian coordinate system, x, y, z and denote the velocity components by u, v, w. The latter are made dimensionless by the critical speed of sound. The other reference property is the critical density. Denoting properties with dimensions with a prime we have the following relations:

$$u = \frac{u'}{a'^*} \qquad v = \frac{v'}{a'^*} \qquad w = \frac{w'}{a'^*}$$

$$\rho = \frac{\rho'}{\rho'^*} \qquad p = \frac{p'}{\rho^* a'^{*2}} = \frac{p'}{\gamma p'^*} \tag{2.1}$$

The flow is assumed to be isoenergetic. Then the constant total enthalpy is given by:

$$H = \frac{h'_t}{a'^{*2}} = \frac{\gamma}{\gamma-1}\frac{p}{\rho} + \frac{1}{2}q^2 = H^* \tag{2.2}$$

where $q^2 = u^2 + v^2 + w^2$ and

$$H^* = \frac{1}{\gamma-1} + \frac{1}{2} = \frac{\gamma+1}{2(\gamma-1)}$$

Then we write the differential equation in the following conservation form:

$$W_x = F_y + G_z \tag{2.3}$$

Here, W is a column vector with four elements, the transpose of which is

$$W^T \equiv \left\{W_1, W_2, W_3, W_4\right\}$$

$$= \left\{\rho u, \rho u^2 + p, \rho uv, \rho uw\right\}$$

Similarly, the transpose of the vectors F and G are given by:

$$- F^T = \left\{\rho v,\ \rho uv,\ \rho v^2 + p,\ \rho vw\right\}$$

$$- G^T = \left\{\rho w,\ \rho uw,\ \rho vw,\ \rho w^2 + p\right\} \tag{2.5}$$

Considering the elements of W to be the dependent variables we find that the elements of F and G can be expressed in terms of the elements of W. It is necessary to evaluate for example ρ from a quadratic equation,

$$\rho = A^{-1}\left[B \mp \sqrt{B^2 - AC}\right] \tag{2.6}$$

where:

$$A = 2H^* - \left(W_3/W_1\right)^2 - \left(W_4/W_1\right)^2$$

$$B = \gamma(\gamma-1)^{-1} W_2$$

$$C = (\gamma+1)(\gamma-1)^{-1} W_1^2$$

It is easily verified that $B^2 = AC$ at sonic conditions. Then, the upper or lower sign in Eq. (2.6) correspond to supersonic and subsonic flows respectively.

3. The Difference Scheme

In order to describe the difference approximation to Eq. (2.3) we introduce the following notation: The difference approximation to $W(x + \ell\Delta x, y + m\Delta y, z + n\Delta z)$ is denoted by $W^{\ell}_{m,n}$. Since W is strictly defined only on the grid points, ℓ, m and n are considered to be integers. However, values of W can be defined at points intermediate by interpolation formulae. We will indicate this by writing the difference approximation to the p^{th}-order derivative ($p \geq o$) as follows:

$$\left.\frac{\partial^p W}{\partial y^p}\right|_{\lambda,\mu,\nu} = \left\langle \frac{\partial^p W}{\partial y^p} \right\rangle^{\lambda}_{\mu,\nu} \tag{3.1}$$

where λ, μ, ν give the location where the derivative is taken corresponding to ℓ, m, n. However, the greek symbols are not necessarily integers.

On occasion we will extend the notation in Eq. (3.1) by indicating half the interval, q, over which the difference approximation is taken. In this case we write

$$\left.\frac{\partial^p W}{\partial y^p}\right|_{\lambda,\mu,\nu} = \left\langle \frac{\partial^p W}{\partial y^p} /q \right\rangle^{\lambda}_{\mu,\nu} \tag{3.1a}$$

Now we define these approximations as follows:

$$\langle W/\tfrac{1}{2}\rangle^{\ell}_{\pm\frac{1}{2},n} = \frac{1}{2}\left[W^{\ell}_{\pm1,n} + W^{\ell}_{o,n}\right] \tag{3.2a}$$

$$\left\langle \frac{\partial W}{\partial y}/q \right\rangle^{\lambda}_{\mu,n} = \frac{1}{2q\Delta y}\left[W^{\lambda}_{\mu+q,n} - W^{\lambda}_{\mu-q,n}\right] \tag{3.2b}$$

$$\left\langle \frac{\partial W}{\partial y}/1 \right\rangle^{\ell}_{o,\pm\frac{1}{2}} = \frac{1}{2}\left[\left\langle \frac{\partial W}{\partial y}/1 \right\rangle^{\ell}_{o,o} + \left\langle \frac{\partial W}{\partial y}/1 \right\rangle^{\ell}_{o,\pm 1}\right]$$

$$= \frac{1}{4\Delta y}\left[W^{\ell}_{+1,o} - W^{\ell}_{-1,o} + W^{\ell}_{+1,\pm 1} - W^{\ell}_{-1,\pm 1}\right] \qquad (3.2c)$$

Derivatives with respect to z are approximated similarly by operating on the second subscript. Finally, the function $F(W^{\lambda}_{\mu,\nu})$ are denoted by $F^{\lambda}_{\mu,\nu}$ and similar for G.

Now the difference approximation to Eq. (2.3) is based on the Taylor expansion of W in x-direction, i.e.

$$W(x+\Delta x,y,z) = W(x,y,z) + \Delta x\, W_x(x,y,z) + \frac{\Delta x^2}{2} W_{xx}(x,y,z) + O(\Delta x^3) \qquad (3.3)$$

With the notation introduced above, Eq. (3.3) is approximated by:

$$W^{1}_{o,o} = W^{o}_{o,o} + \Delta x \langle W_x \rangle^{o}_{o,o} + \frac{\Delta x^2}{2} \langle W_{xx} \rangle^{o}_{o,o} \qquad (3.4)$$

The terms on the right hand side are calculated in two steps as follows:

i) First step: Calculate temporary values

$$\langle \bar{W} \rangle^{\pm\frac{1}{2}}_{\pm\frac{1}{2},o} \text{ and } \langle \bar{W} \rangle^{\pm\frac{1}{2}}_{o,\pm\frac{1}{2}}$$

to first order accuracy.

These temporary values are based on Taylor expansions of W about the points $(x,y \pm \frac{\Delta y}{2}, z)$ and $(x,y,z \pm \frac{\Delta z}{2})$ respectively. The difference approximations to these Taylor series are:

$$\langle \bar{W} \rangle^{\pm\frac{1}{2}}_{\mu,\nu} = \langle W/\tfrac{1}{2} \rangle^{o}_{\mu,\nu} \pm \frac{\Delta x}{2} \langle W_x \rangle^{o}_{\mu,\nu} \qquad (3.5)$$

The x-derivative in Eq. (3.5) is replaced by introducing the differential equation:

$$\langle W_x \rangle^{o}_{\mu,\nu} = \langle F_y \rangle^{o}_{\mu,\nu} + \langle G_z \rangle^{o}_{\mu,\nu}$$

In particular we obtain:

$$\langle W_x \rangle^{o}_{\pm\frac{1}{2},o} = \langle F_y/\tfrac{1}{2} \rangle^{o}_{\pm\frac{1}{2},o} + \langle G_z/1 \rangle^{o}_{\pm\frac{1}{2},o}$$

$$= \frac{\pm 1}{\Delta y}\left[F^{o}_{\pm 1,o} - F^{o}_{o,o}\right] + \frac{1}{4\Delta z}\left[G^{o}_{o,+1} - G^{o}_{o,-1} + G^{o}_{\pm 1,+1} - G^{o}_{\pm 1,-1}\right]$$

and similarly for the other terms. Based on these temporary values we calculate the following eight properties

$$F^{\pm\frac{1}{2}}_{\pm\frac{1}{2},o} \text{ and } G^{\pm\frac{1}{2}}_{o,\pm\frac{1}{2}}$$

ii) Second step: Evaluate $\langle W_{xx} \rangle^{o}_{o,o}$ using the temporary values at $\lambda = \pm\frac{1}{2}$ and $\langle W_x \rangle^{o}_{o,o}$.

Making use again of the differential equation, the second order term in the Taylor series, Eq. (3.4), is calculated from:

$$\langle W_{xx} \rangle^{o}_{o,o} = \frac{1}{\Delta x}\left[\langle W_x \rangle^{+\frac{1}{2}}_{o,o} - \langle W_x \rangle^{-\frac{1}{2}}_{o,o}\right]$$

$$= \frac{1}{\Delta x}\left[\langle F_y/\tfrac{1}{2} \rangle^{+\frac{1}{2}}_{o,o} - \langle F_y/\tfrac{1}{2} \rangle^{-\frac{1}{2}}_{o,o}\right. \qquad (3.6)$$

$$\left. + \langle G_z/\tfrac{1}{2} \rangle^{+\frac{1}{2}}_{o,o} - \langle G_z/\tfrac{1}{2} \rangle^{-\frac{1}{2}}_{o,o}\right]$$

Hence, for example:

$$\langle F_y/\tfrac{1}{2} \rangle^{\pm\frac{1}{2}}_{o,o} = \frac{1}{\Delta y}\left[F^{\pm\frac{1}{2}}_{+\frac{1}{2},o} - F^{\pm\frac{1}{2}}_{-\frac{1}{2},o}\right] \text{ etc.}$$

Again using the differential equation, the remaining term in the Taylor expansion is obtained:

$$\langle W_x \rangle^{o}_{o,o} = \langle F_y/1 \rangle^{o}_{o,o} + \langle G_z/1 \rangle^{o}_{o,o} \tag{3.7}$$

Introducing Eqs. (3.6) and (3.7) into Eq. (3.4) yields the final value $W^{1}_{o,o}$.

It is easily verified, that the difference scheme described above is accurate to order Δ^2, where Δ stands for Δx, Δy or Δz which are all considered to be of the same order of magnitude. For the sake of simplicity we assume $\Delta y = \Delta z$ and introduce the relative step size λ by

$$\lambda = \Delta x/\Delta y \tag{3.8}$$

we then observe, that the first and second order terms in the Taylor series, Eq. (3.4), are proportional to λ and λ^2 respectively.

The stability of this new difference scheme is the same as for the two-step Lax-Wendroff scheme used in Ref. 1. It is, therefore, given by:

$$\lambda \leq C \cot (|\theta| + \mu) \tag{3.9}$$

where $C^2 = 3/8$, θ is the angle between the velocity vector and the x-axis and μ is the Mach angle. Now the allowable step size λ varies according to Eq. (3.9) in the flowfield. We denote by Λ the relative step size actually used to advance the solution one step. In order not to violate the stability condition anywhere in the flowfield, Λ is determined by:

$$\Lambda = \min \left\{ \lambda_{\ell oc}(y,z) \right\} \tag{3.10}$$

Here, $\lambda_{\ell oc}$ is the local value of λ, determined by using the equality sign in Eq. (3.9), i.e.

$$\lambda_{\ell oc} = C \cot (|\theta| + \mu) \tag{3.9a}$$

Thus, as given in Eq. (3.10), Λ is the smallest value of all the $\lambda_{\ell oc}$ in the x = constant plane.

Now in highly nonuniform flowfields, such as are encountered in the present application, the value of Λ can become very small. For high Mach numbers (i.e. small μ) it is usually the flow angle θ which determines the allowable step size Λ.

If Λ is small, then the second order term in the Taylor expansion, Eq. (3.4) becomes very small indeed, being of order Λ^2. Since it is this second order term which is responsible for the damping of the oscillations observed behind shock waves, a small value of Λ can be expected to yield very pronounced oscillations. This has been observed in Ref. 1.

We now consider a modified difference scheme which differs from the above by the introduction of a damping parameter, D, which multiplies the second order term. Introducing further the relative step size λ we have:

$$W^1_{o,o} = W^o_{o,o} + \lambda \left[\Delta y \, \langle W_x \rangle^o_{o,o}\right] + \frac{1}{2} D\lambda^2 \left[\Delta y^2 \, \langle W_{xx} \rangle^o_{o,o}\right] \tag{3.10}$$

We have used the assumption $\Delta y = \Delta z$. The terms in square brackets are calculated as given above. If $D = 1 + O(\Delta)$, then the accuracy is the same as above i.e. of $O(\Delta^2)$. If D is larger, the accuracy is reduced to first order.

The influence of the factor D on the stability has been studied in Ref. 2. It was found that the difference scheme, Eq. (3.10), is stable if

$$\begin{aligned} \lambda &\le D^{-\frac{1}{2}} C' \cot\left(|\theta| + \mu\right) \\ &\le D^{-\frac{1}{2}} \lambda'_{\ell oc} \end{aligned} \tag{3.11}$$

In this case, $C'^2 = \frac{1}{2}$, which is slightly larger than the value given in Eq. (3.9). Equation (3.11) shows, that for $D > 1$ the allowable step size is reduced.

We now discuss two different methods of damping. The first, called uniform damping, uses the same damping factor at each point of the plane x = constant, but not necessarily the same in each plane. The second method, called local damping, will use a different D at each point in the plane x = constant.

Of the two methods, the first has been subjected to a considerable number of tests, using a simple two-dimensional problem, while the results of the second method are rather sketchy. Nevertheless, for reasons to be explained below, it is the second method which has been incorporated in the program for the five jet interaction flowfield calculation.

4. Uniform Damping

The simplified test problem considered in this and the next section is that of the flow through an oblique shock wave (Fig. 1). All properties ahead of and behind the shock are denoted by the subscripts 1 and 2 respectively, (Fig. 1A). The flow ahead of the shock is assumed to be inclined towards the x-axis by an angle δ. It is deflected by the shock through this angle parallel to the x-axis.

Figure 1B shows an idealized smeared out shock. Since the marching step Δx will depend on the difference scheme used, we use the lateral step size Δy as a reference length. We expect that we cannot do better with the finite difference scheme than to smear the shock over a thickness Δy normal to the shock front. Hence, we will compare our numerical solution to this idealized shock thickness, $s = x_2 - x_1 = \Delta y/\sin(\theta - \delta)$.

In Fig. 1C we show the expected distributions of any quantity, ϕ, along a line y = constant. The theoretical distribution in the discontinuous function

$$\phi_{th} = \begin{cases} \phi_1 & x < x_1 \\ \phi_2 & x > x_1 \end{cases} \tag{4.1}$$

The idealized smeared out shock is characterized by the distribution

$$\phi_i = \begin{cases} \phi_1 & x \le x_1 \\ \phi_1 + \dfrac{x - x_1}{s}(\phi_2 - \phi_1) & x_1 \le x \le x_2 \\ \phi_2 & x \ge x_2 \end{cases} \tag{4.2}$$

The numerical solution is denoted by ϕ. As is indicated in Fig. 1C, we will in general expect ϕ to oscillate around ϕ_{th}. A measure for the quality of the numerical solution is the shaded area in Fig. 1C, the square of which is given by

$$I(x) = \int_{o}^{x} (\phi - \phi_{th})^2 \, dx \tag{4.3}$$

the integration being taken along a line y = constant.

We now return to our first method of damping which we call uniform damping. In general, the right running characteristic ahead of the shock will be steeper than either characteristics behind the shock, i.e., usually

$$\mu_1 + \delta > \mu_2$$

Since $\delta = |\theta|$, this means that the locally allowed λ'_{loc} in front of the shock is smaller than that based on the condition behind the shock. Denoting the former by λ'_1 we then have the condition that:

$$\Lambda = \lambda'_1$$

Assume now, that we perform a calculation with the maximum allowed step size, i.e. $\Delta x = \Lambda \Delta y$. Then, in the region ahead of the shock,

we must assign the value D = 1 to the damping constant in order that the stability condition is satisfied in this region (see Eq. (3.11)). Alternatively, if we want to use a damping factor D > 1, constant in the flow field, then we have to reduce the step size Λ to Λ' say, where

$$\Lambda' = \eta\Lambda \qquad \eta \leq 1 \tag{4.4}$$

In order not to violate the stability condition in the region ahead of the shock we must have from Eq. (3.11)

$$D \leq \eta^{-2} \tag{4.5}$$

The procedure then was as follows: We selected a number of cases of Mach number and deflection angles. For each of these cases a number of examples were calculated with various damping factors. The step size Λ' was calculated from the stability condition. For each example, the error integrals I (Eq. (4.3)) were evaluated for the properties ϕ = p, ρ, u, and $q = (u^2 + v^2)^{\frac{1}{2}}$. From these error integrals, the optimum damping factor was selected as that which yields the smallest errors.

The results of a number of cases are shown in Figs. 2 to 9. In each figure the pressure distribution along the surface, y = 0, and along y = 2Δy are given for a calculation with D = 1 and a D close to the optimum value. Also indicated is the linear distribution for the ideally smeared shock defined in Eq. (4.2).

In Figs 2 to 4 the Mach number is $M_1 = 3$ and the deflection angle increases from 20° to 35°. Correspondingly, the shock strength increases; a measure for the shock strength is the theoretical pressure ratio across it: $\xi = p_2/p_1$. Alternatively we use

$$\xi' = \frac{\xi - 1}{\xi} = \frac{p_2 - p_1}{p_2}$$

which varies between zero for zero deflection and one for infinite shock strength. For the examples in Fig. 2 to 4 the shock strength varies between $\xi = 3.23$ ($\xi' = 0.69$) and 6.28 (0.84). For the weakest shock, Fig. 2, the oscillations with D = 1 are not very pronounced but for the strongest shock, Fig. 4, they are very considerable. It should in this connection be remembered, that the case D = 1 was calculated with the largest step size allowed. The oscillations would be further increased if the allowable step size were reduced for example, because of a cross flow component such as is the case in the three dimensional interaction regions. The figures demonstrate the considerable improvement which can be obtained especially for the stronger shocks with this damping method. It is also seen, that the shock thickness is not much worse than for the ideally smeared shock.

Similar results are shown in Figs. 5 to 7 for $M_1 = 5.0$ and deflection angles $\delta = 20^\circ$, 30° and 40°. For these cases, the pressure ratio varies between $\xi = 5.82$ ($\xi' = 0.83$) and 16.20 (0.94). Finally, Fig. 8 shows a

case with $M = 7.0$, $\delta = 30^{\circ}$ and $\xi = 18.4$ ($\xi' = 0.946$).

The last two figures show a pronounced pressure undershoot ahead of the shock. For higher Mach numbers this undershoot becomes negative and the numerical procedure breaks down. It is gratifying to see that this undershoot is less critical for $D > 1$ than for $D = 1$. Thus, the introduction of the damping factor delays this breakdown, i.e., it allows calculations with somewhat larger Mach numbers.

Figure 12 shows a summary of these results, i.e., the η for the optimum damping as a function of ξ'. It is seen, that the results can be fairly well correlated by

$$\eta = \sqrt{1 - \xi'^2} \tag{4.6}$$

The point which deviates most from this formula is the case which gives the best result, namely that shown in Fig. 4. These pressure distributions show no noticeable overshoot at all. Consequently, the values of η according to Eq. (4.6) are probably somewhat too large, i.e., the damping factor can be chosen somewhat larger than on the basis of Eq. (4.6). This equation yields

$$D = \frac{1}{1 - \xi'^2} = \frac{\xi^2}{2\xi - 1} \tag{4.7}$$

We notice, that for very strong shocks, $\xi \gg 1$, the damping factor must also become very large:

$$D \doteq \frac{1}{2} \xi$$

The method described above is quite effective, but it has the disadvantage that the damping factor is strongly dependent on the physical conditions, in our example on the pressure ratio across the shock. It has the further disadvantage, that the step size has to be reduced in order to apply damping. This means, of course, that the calculation becomes more expensive.

Consequently, we have tested another damping method which will now be discussed.

5. Local damping.

Consider again the problem of an oblique shock as shown in Fig. 1. Assume that the calculation has proceeded to a line x = constant, such that there are some points near y = 0 ($y < y_1$, say) with properties near the condition behind the shock and some, at larger y ($y > y_1$) with essentially data ahead of the shock. Thus, the allowable relative step size for D = 1 is

$$\lambda_1 \text{ for } y > y_1$$

$$\lambda_2 \text{ for } y < y_1.$$

Again, $\lambda_2 > \lambda_1$, depending on the Mach number and deflection angle.

Consequently, the solution can be advanced according to λ_1, i.e.,

$$\Lambda = \lambda_1.$$

However, for this value of the step size, the stability criterion allows in the region $y < y_1$ behind the shock use of a damping factor D larger than one. It can be chosen of the order $(\lambda_2/\lambda_1)^2$. Therefore, for more general cases, we proceed as follows: At each station x = constant, the locally allowable step size λ_{loc} is calculated and the minimum is determined:

$$\Lambda = \min \left\{ \lambda_{loc} (y,z) \right\} \tag{5.1}$$

The solution is then advanced according to this step size, but at each point a damping factor of

$$D(y,z) = \epsilon \, (\lambda_{loc}/\Lambda)^{\nu} \tag{5.2}$$

is used where $\nu \leq 2$.

This procedure was tested on an example, somewhat more critical than those reported in the last section. Again, an oblique shock problem was used but the minimum allowable step size $\Lambda = \lambda_1$ was artificially reduced in x-direction according to an exponential law. The results are shown in Figs. 10 and 11.

Figure 10 shows the influence of this artificial decrease in step size if no additional damping is used, i.e., for $D = 1$. Λ was reduced by about a factor of 1/3 over the range shown in the figure, i.e., at $x = 0$ the step size was about three times larger than at the right-hand side of the graph. It is remembered that in the jet interaction regions the allowable step size is much more drastically reduced because of the cross flow components. However, Fig. 10 shows that even this mild reduction in step size has a strong adverse effect on the results, in the sense that the oscillations are not only more pronounced but in addition are very poorly damped, if at all. It is quite likely that a more rapid reduction on Λ will result in oscillations with increasing amplitude. It is interesting to note that the frequency of the oscillations is not materially affected by the decrease in step size.

In Fig. 11 the results with the local damping factor according to Eq. (5.2) are shown. Two experiments were conducted with $\epsilon = 1$ and 1/2, $\nu = 2$.

Consider first the pressure distribution along the wall. It is seen that the introduction of the damping factor increases the initial pressure rise through the shock. If ϵ is too large, i.e., one in this case, this results in an overshoot and subsequent strongly damped oscillation. Reduction of ϵ to half the value practically eliminates the overshoot. However, a small residual oscillation of longer wave lengths is observed far downstream.

Off the surface, the curve with $\epsilon = 1$ shows slightly better results than $\epsilon = 1/2$ from the point view of oscillation of the solution. However, the steepness of the pressure gradient is somewhat reduced for the larger ϵ.

In comparing Fig. 11 with the results obtained with uniform damping, Fig. 6, it is noticed that the latter is of somewhat better quality. This, of course, is partially caused by the artificial decrease of the step size in Fig. 11.

It is interesting to note that with this damping method the shock wave at the surface is smeared out less than the ideally smeared out shock.

6. Application to the Jet-Interaction Program.

The damping method of the last section has been incorporated into the five-jet interaction program described fully in Ref. 1. The results of a sample calculation are presented in Figs. 12 to 13.

In Ref. 1, the step size Δx was artificially increased by ignoring the right running characteristics ahead of the shock. Referring to Fig. 1, this means that the relative step size ahead of the shock was calculated on the basis of the left running characteristic only, i.e.,

$$\lambda''_{\ell oc} = C \cot(\delta - \mu'_1).$$

This had the effect that the smallest allowable step size, Λ, was obtained in the region behind the shock, i.e., $\Lambda = \lambda_2$. Although this is, of course, theoretically not permissible, no instabilities were observed with this method. The reason for this is presumably that the signals travelling along the ignored characteristics were swallowed by the shock long before they could be amplified sufficiently to lead to instabilities. On the other hand, it is not certain whether results obtained in this fashion cannot be falsified severely by this trick, since the problem is mathematically not well posed any more.

This artificial device has now been abandoned. The step sizes with which the present results have been calculated are, therefore, considerably smaller than those used in Ref. 1. Nevertheless, the pressure distributions in Fig. 12 are of the same quality as the best obtained in Ref. 1.

The results were obtained with $\epsilon = 3/4$, which seems to be a reasonable value for most cases. Figure 12 shows that the pressure rise is again steeper

than for the ideally smeared shock in the interaction plane. For the test examples, the locally used damping factors were printed out and it was found that they were as large as 25. This means that behind the shock, the step size was nearly six times smaller than was locally allowed. This was mostly caused by the large cross flow components in the region ahead of the shock, i.e., in the axisymmetric portion of the jets.

In Fig. 13, a relief is shown for the pressure distribution in the interaction plane $y = 0$. This figure can be compared with that given in Ref. 3. There the interaction of two cylindrical jets has been calculated by the method of characteristics. The results of Ref. 3 extend only over about 1/3 of the jet radius in x-direction; those in the present case extend over about 1.5 exit radii. The figure indicates that in our case too the pressure "jump" across the shock increases along the interaction line, although much slower. This is caused by the fact that the deflection angle increases less rapidly in our case because the jet boundary becomes less inclined to the jet axis in downstream direction. The location of the observed pressure maxima is projected onto the x,z-plane. It is located at less than 5 mesh sizes Δz from the theoretical shock location.

It seems to us that the results presented in Figs. 12 and 13 represent useful data for estimating the thermodynamic state of the gas in the interaction region of multiple jets. If desired, the data could be replaced by estimates, such as shown in Fig. 11 making use of the known shock location in the interaction plane. Cross plots of thermodynamic data in a plane $x = \text{constant}$ (see Ref. 1) show the shock location with good accuracy and very sharply defined.

References

1) L. D'Attorre, G. Nowak and H. U. Thommen, "Inviscid Analysis of the Plume Created by Multiple Rocket Engines," Part I, GD/C-DBE-66-014, May 1966.

2) H. U. Thommen and L. D'Attorre, "Calculation of Steady, Three-dimensional Supersonic Flow Fields by a Finite Difference Method," AIAA Paper No. 65-26, 2nd AIAA Aerospace Science Meeting, New York, 1965.

3) C. W. Chu, A. F. Niemann, Jr., S. A. Powers and H. Ziegler, "Interaction of Two Cylindrical Jets," Technical Note, AIAA Journal, Vol. 5, No. 2, 1967.

APPENDIX

Input Card Format

Input Format

Card No.	Variable	Format	Column	Definition
1	IMIN	I10	1-10	No. of first cross plane computed
	IMAX	I10	11-20	No. of last cross plane computed
	MO	I10	21-30	No. of intervals between axis of centerjet and interaction plane
	JUMP1	I10	31-40	No. of cross planes calculated with half the mesh spacing
2	GAM	F10.5	1-10	Ratio of specific heats, γ
	FACTOR	F10.5	11-20	Constant factor for stability calculation, FACTOR $\leq$ 0.57
	RDJ	F10.5	21-30	Half the separation distance of the axis of the two nearest jets
	C1	F10.5	31-40	Tolerance controlling the spread of the three dimensional region towards the center jet.
	C2	F10.5	41-50	Same for spread towards outside jet
	DPRNT	F10.5	51-60	DPRNT = 0.0: Every plane calculated is printed out DPRNT = Δx: Only those planes are printed out which are closest to the multiples of this interval.
	CN	F10.5	61-70	Radius of the initial data line for the single jet
	CXR	F10.5	71-80	Distance between nozzle exit and origin of the polar coordinate system used in the single jet calculation
3	EPS	F10.5	1-10	Damping factor ϵ
	XPN	F10.5	11-20	Damping exponent $\leq$ 2

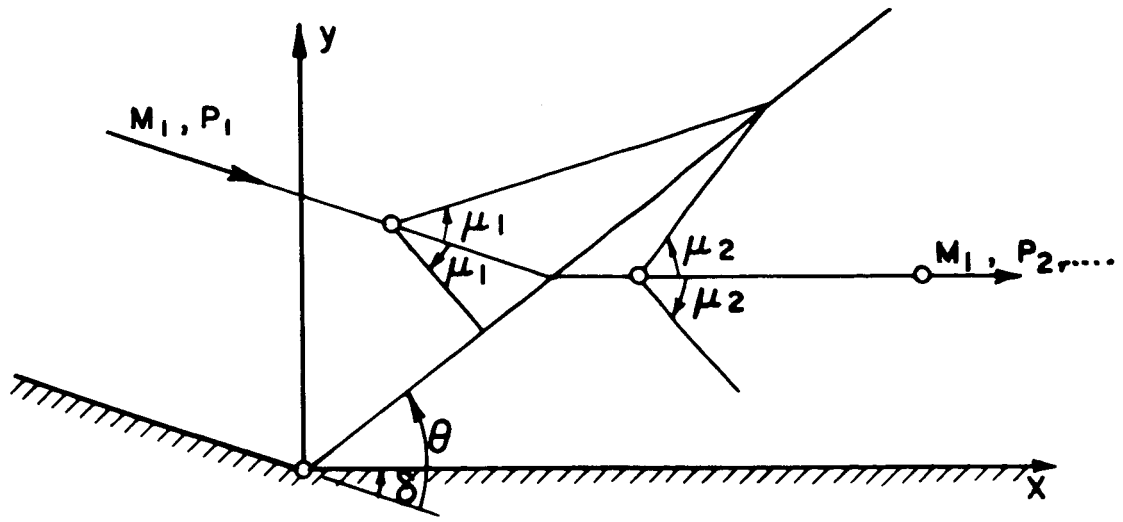

FIG. 1 A : OBLIQUE SHOCK, THEORETICAL

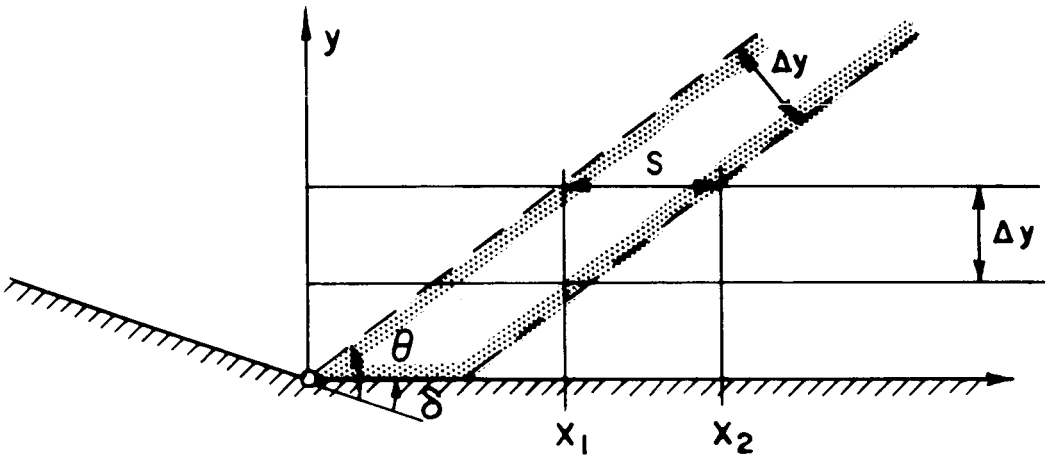

FIG. 1 B : SMEARED OUT SHOCK

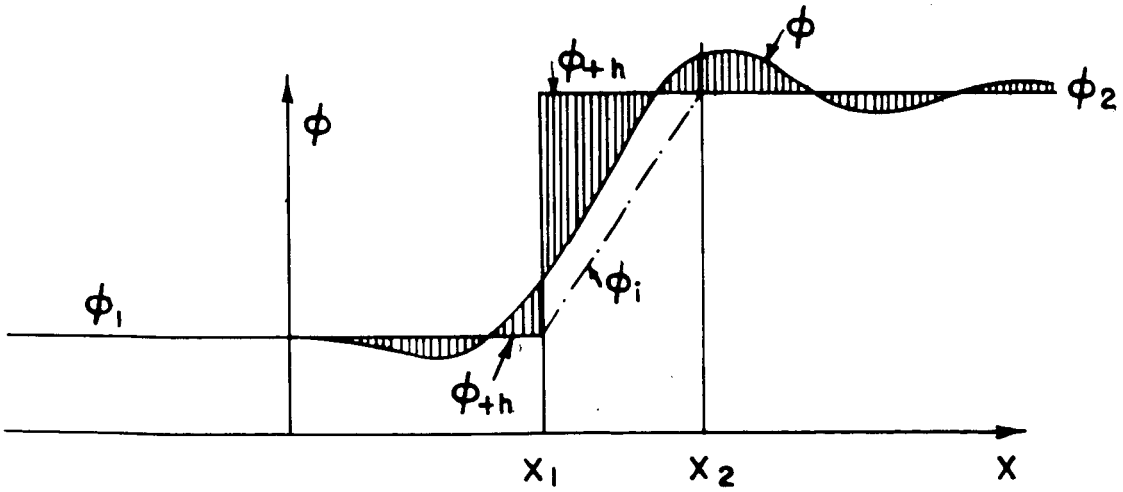

FIG. 1 : THE OBLIQUE SHOCK WAVE PROBLEM

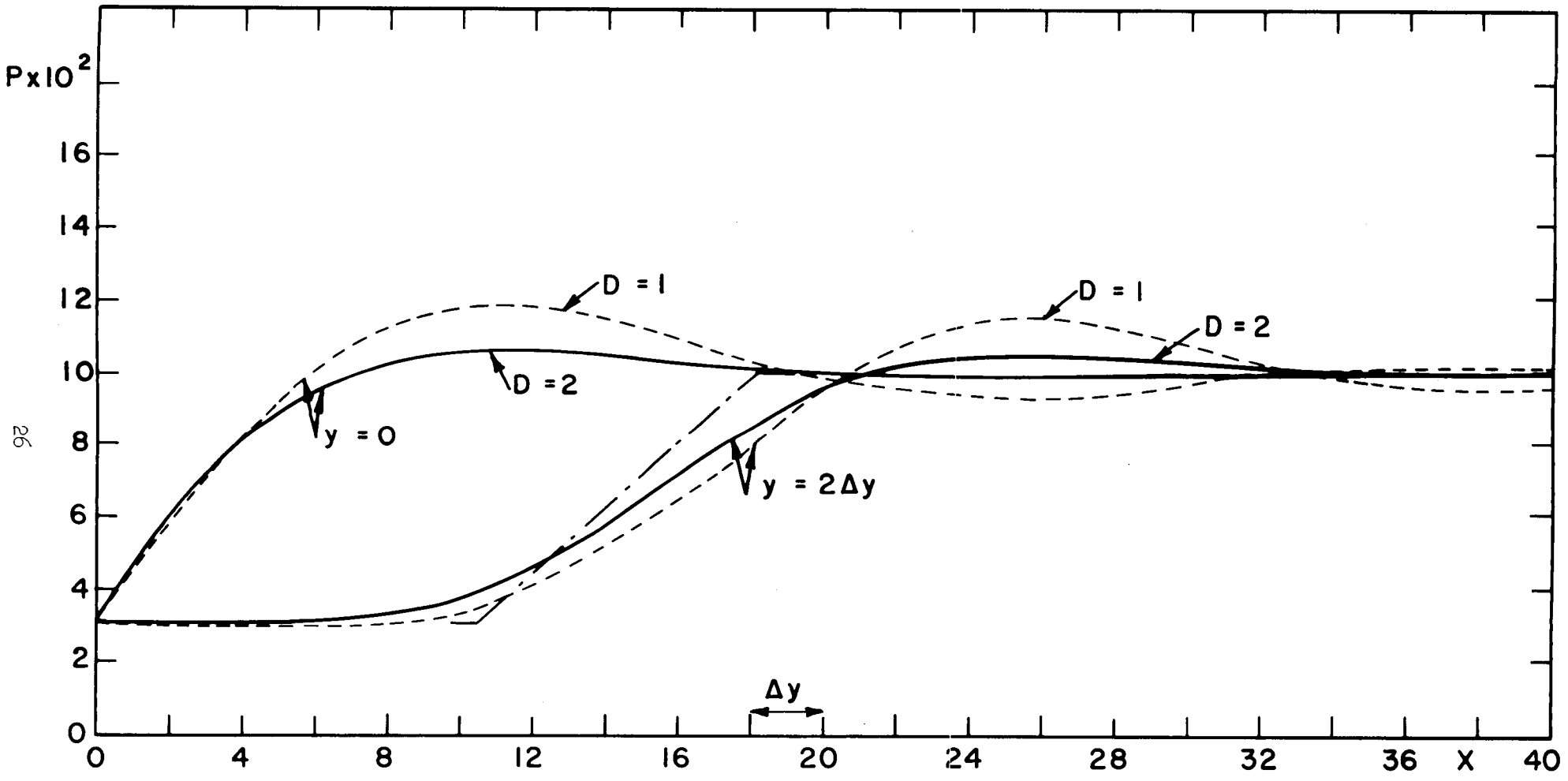

FIG. 2 : PRESSURE DISTRIBUTION THROUGH OBLIQUE SHOCK WITH UNIFORM DAMPING
$M_1 = 3$, $\delta = 20°$, $\gamma = 1.2$

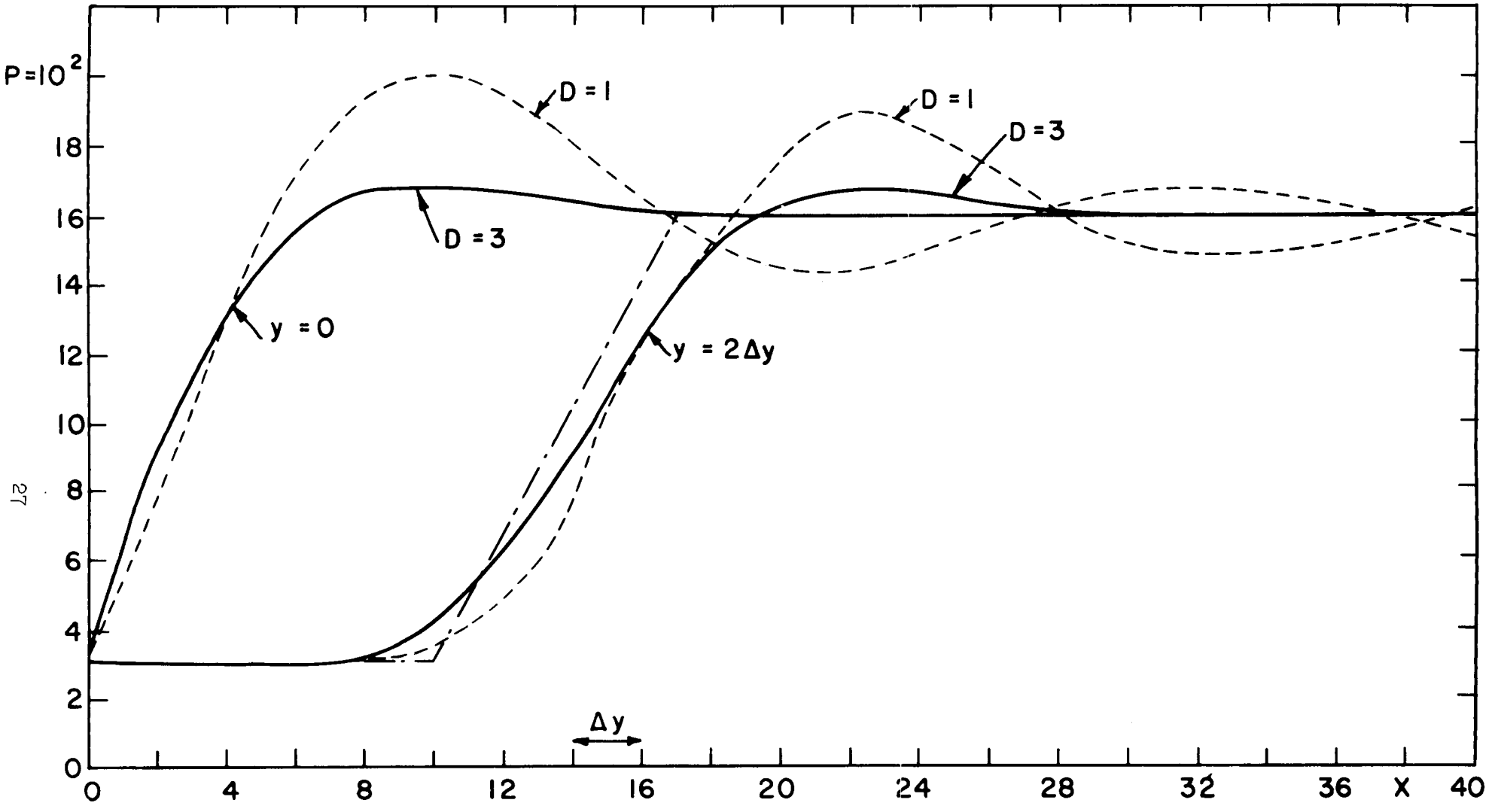

FIG. 3 : PRESSURE DISTRIBUTION THROUGH OBLIQUE SHOCK WITH UNIFORM DAMPING
$M_1 = 3$, $\delta = 30°$, $\gamma = 1.2$

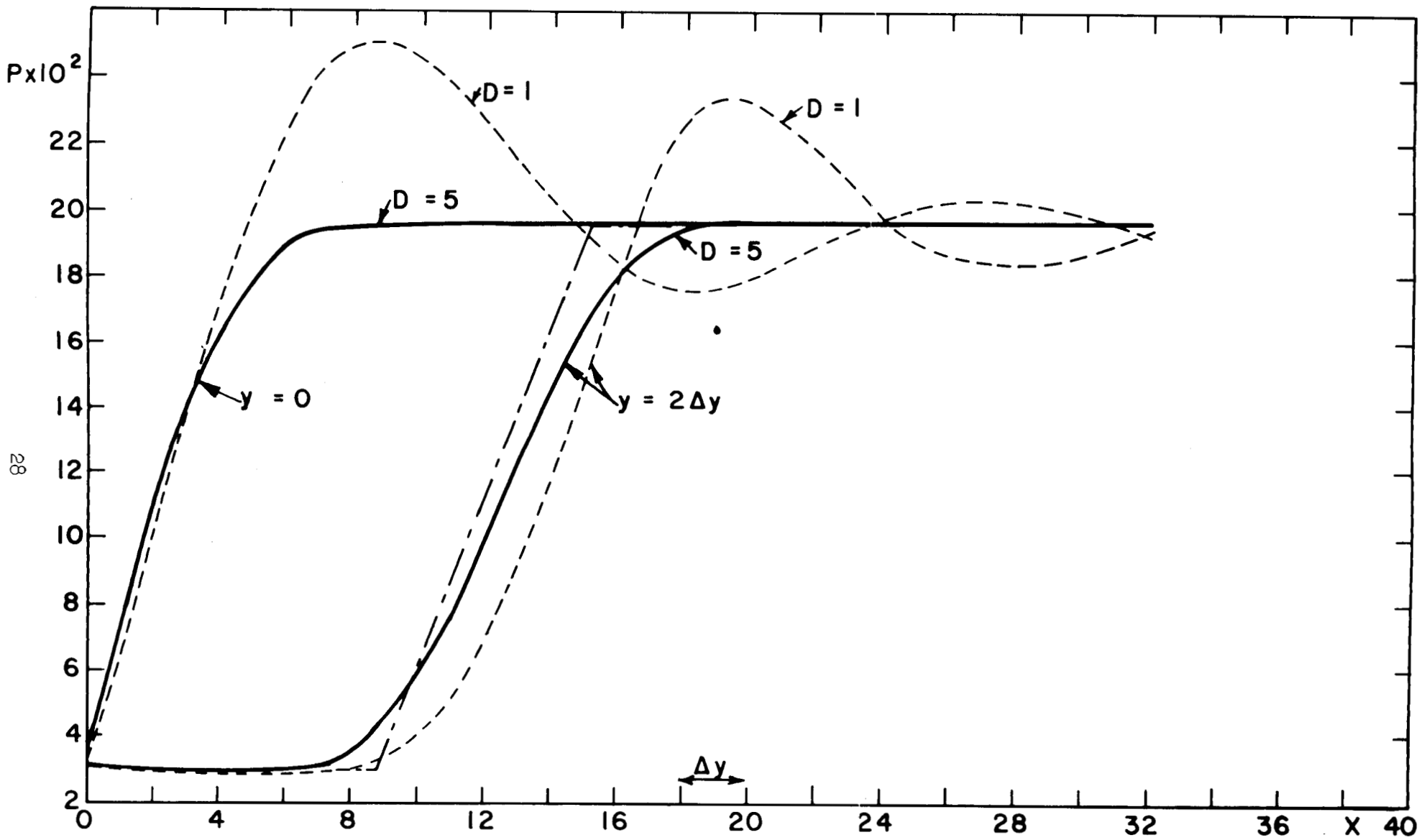

FIG. 4 : PRESSURE DISTRIBUTION THROUGH OBLIQUE SHOCK WITH UNIFORM DAMPING
$M_1 = 3$, $\delta = 35$, $\gamma = 1.2$

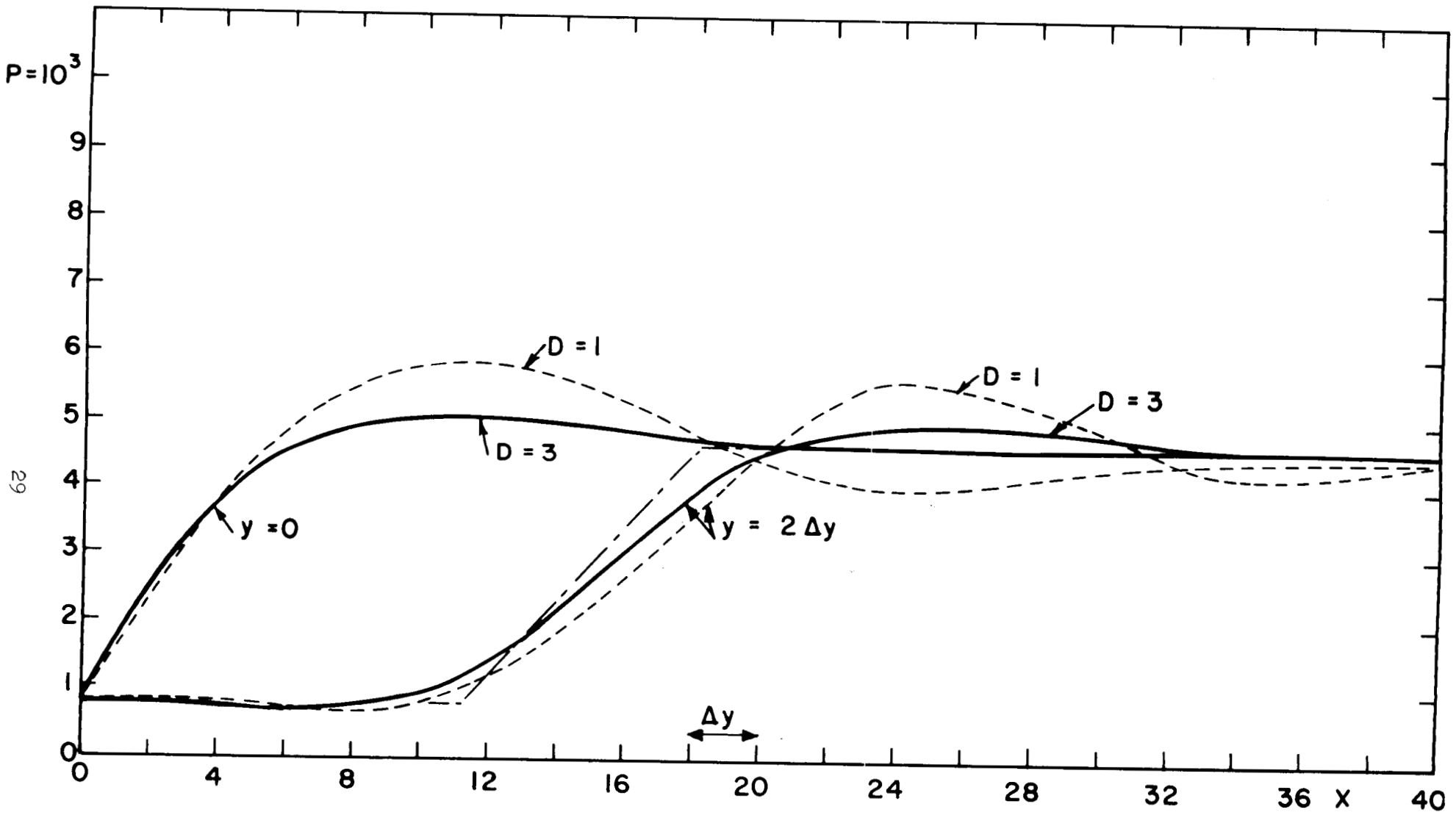

FIG. 5 : PRESSURE DISTRIBUTION THROUGH OBLIQUE SHOCK WITH UNIFORM DAMPING
$M_1 = 5$, $\delta = 20°$, $\gamma = 1.2$

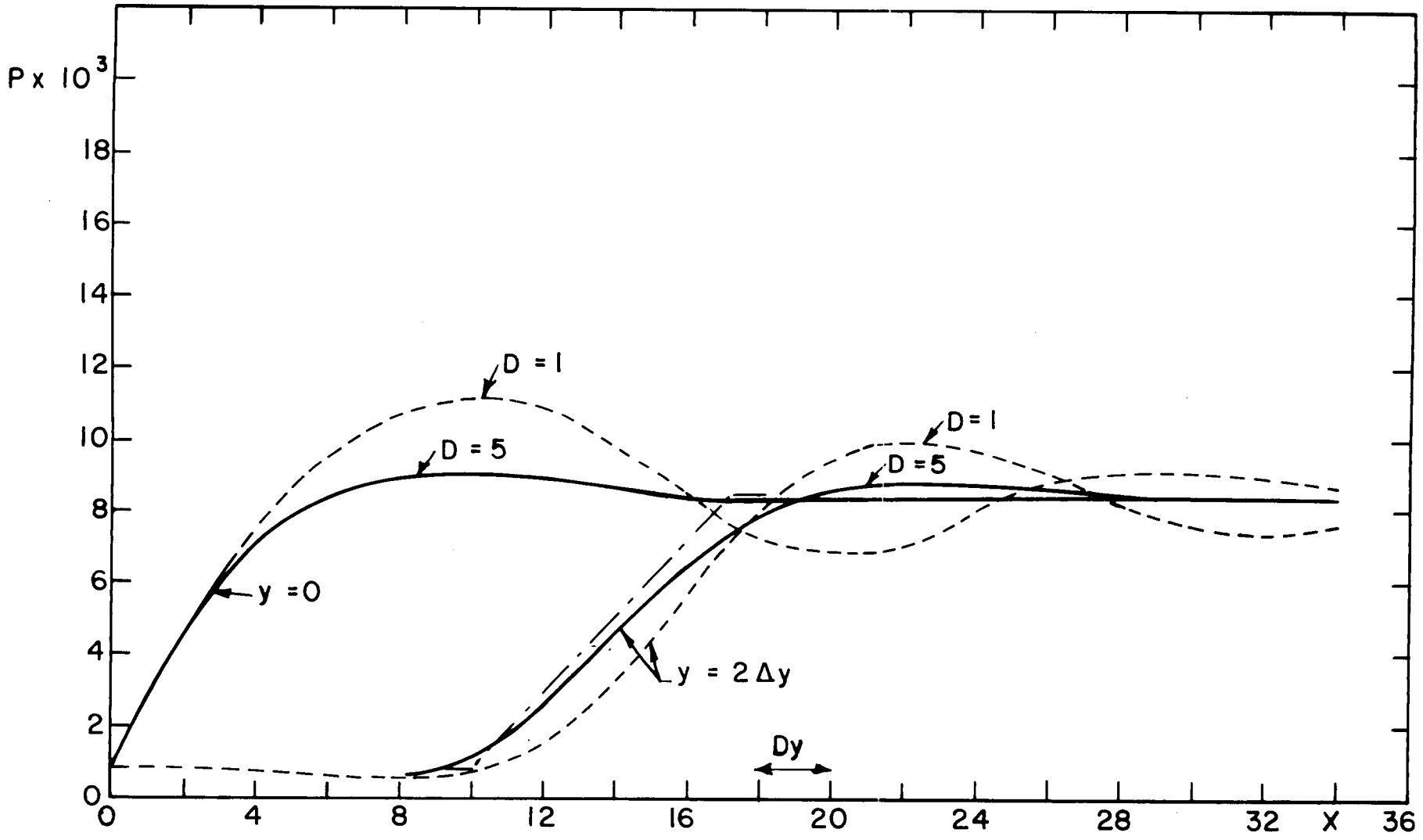

FIG. 6 : PRESSURE DISTRIBUTION THROUGH OBLIQUE SHOCK WITH UNIFORM DAMPING
$M_1 = 5$, $\delta = 30°$, $\gamma = 1.2$

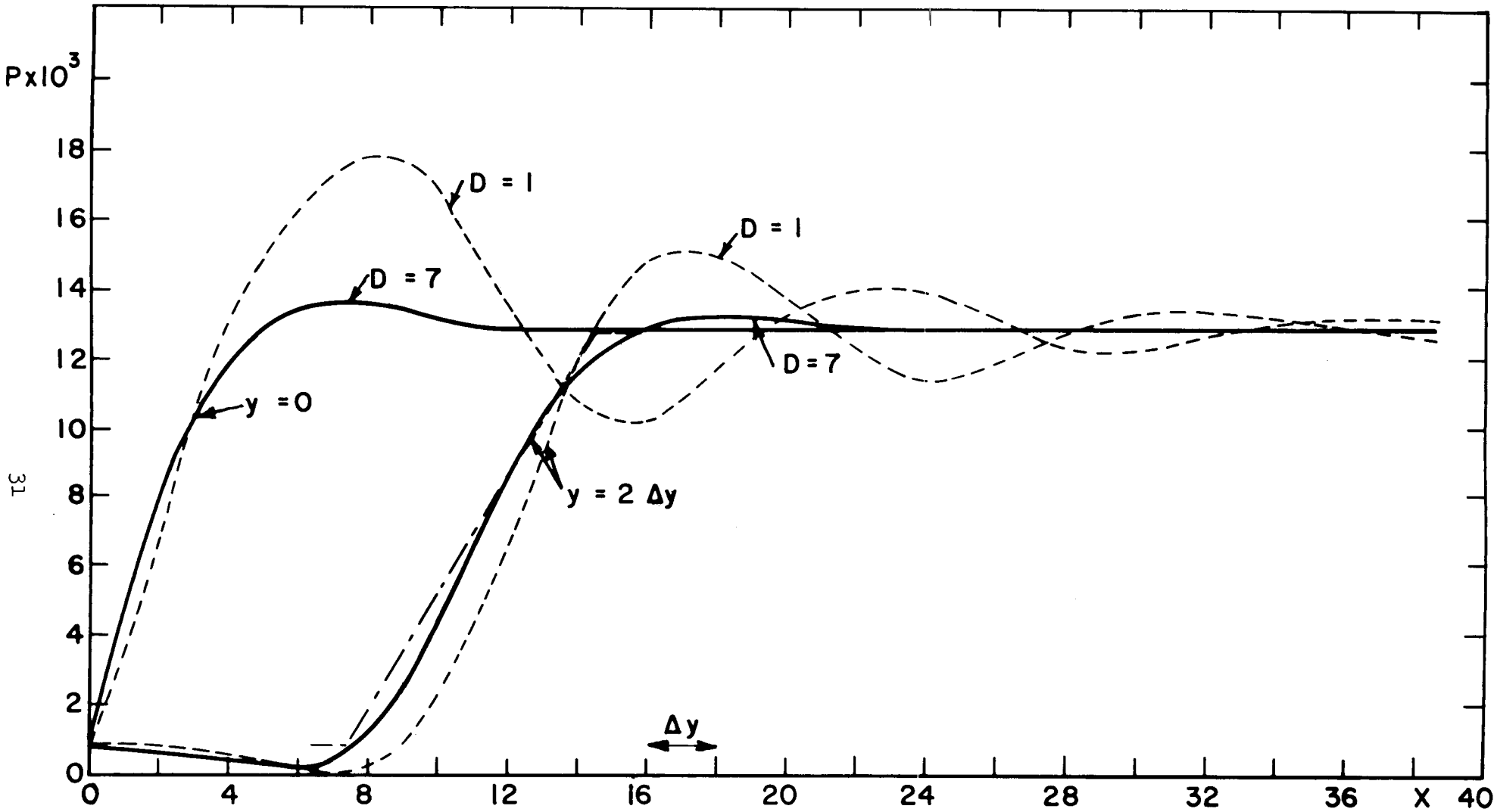

FIG. 7 : PRESSURE DISTRIBUTION THROUGH OBLIQUE SHOCK WITH UNIFORM DAMPING
$M_1 = 5$, $\delta = 40°$, $\gamma = 1.2$

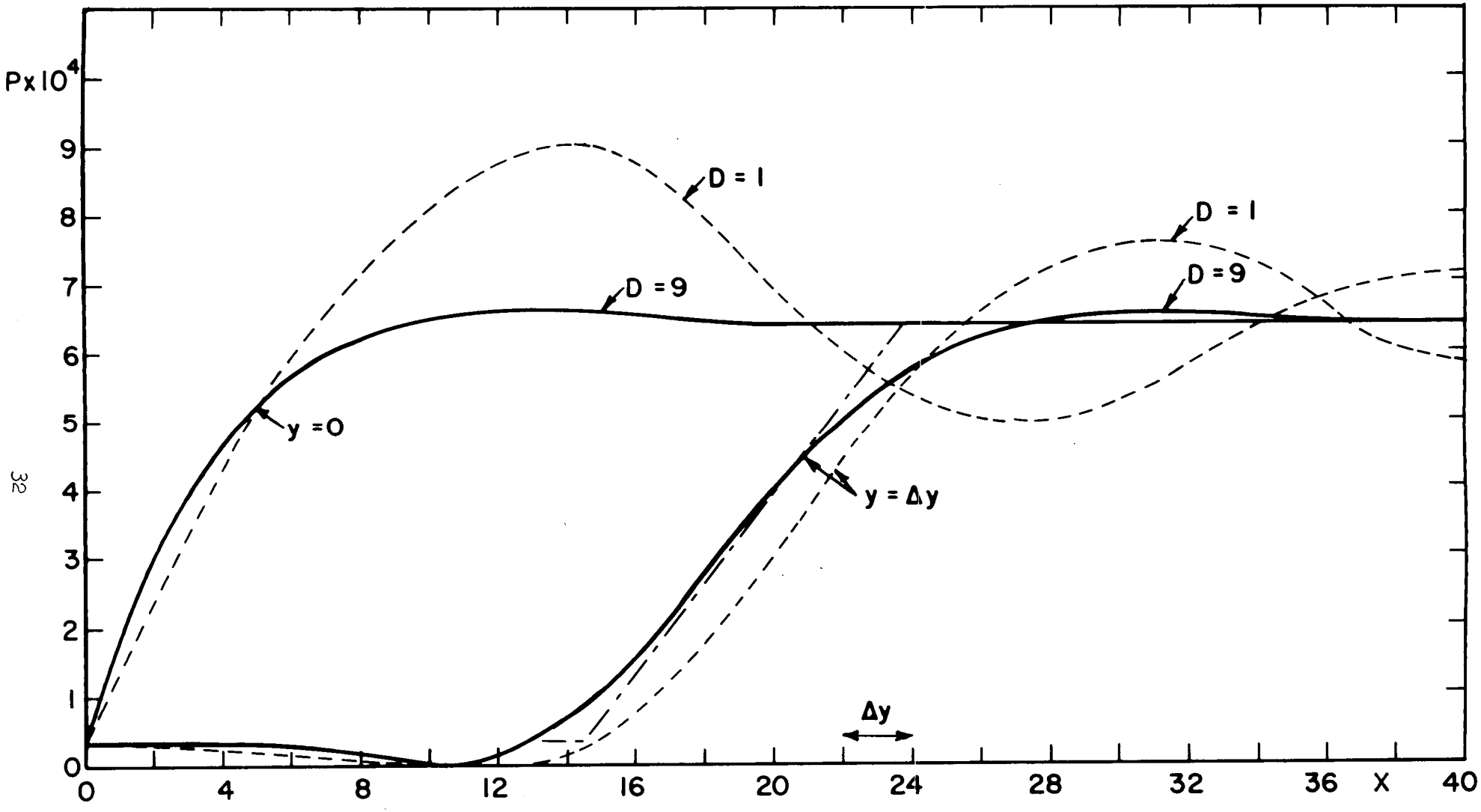

FIG. 8 : PRESSURE DISTRIBUTION THROUGH OBLIQUE SHOCK WITH UNIFORM DAMPING
$M_1 = 7$, $\delta = 30°$, $\gamma = 1.2$

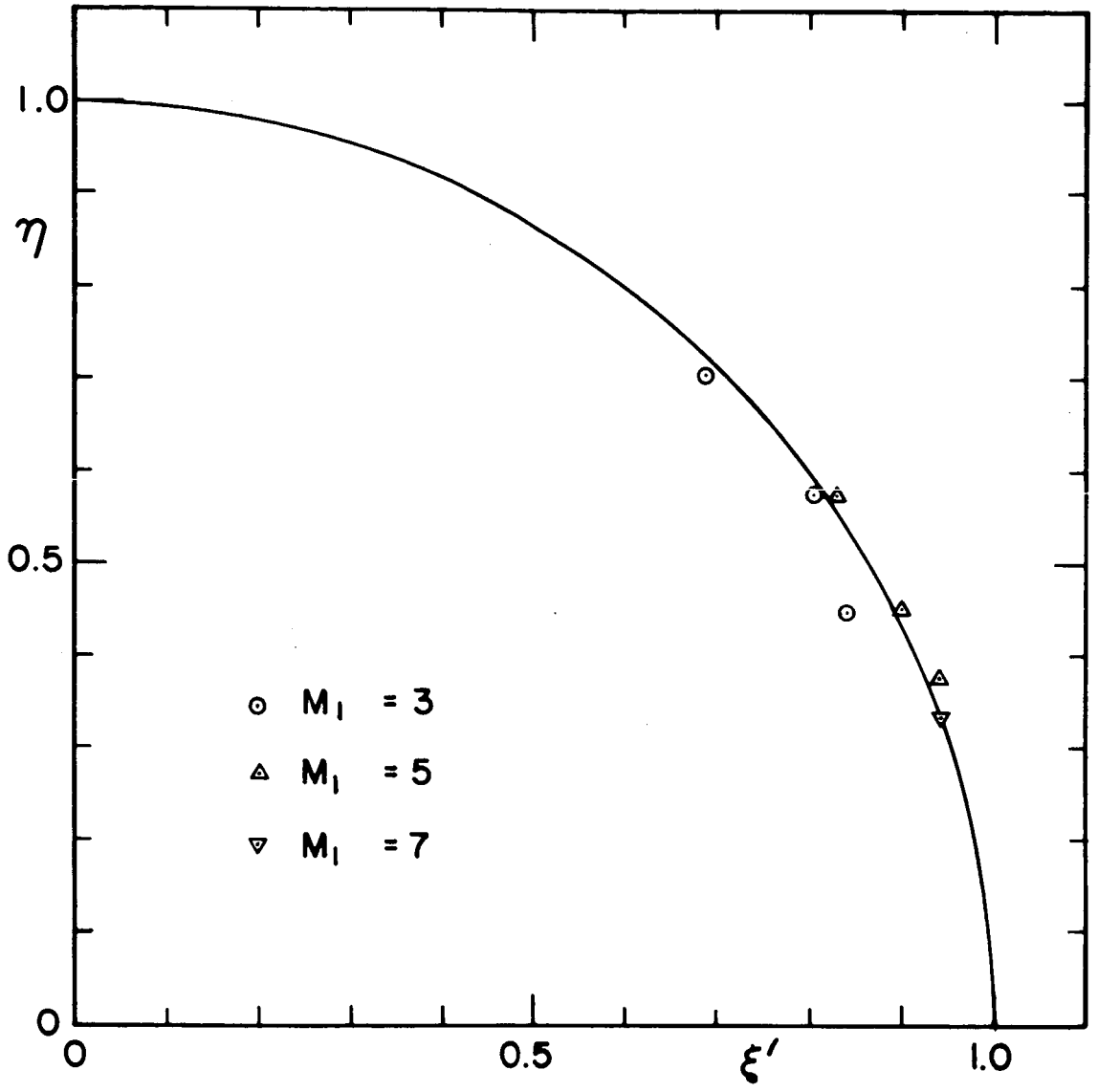

FIG. 9 : CORRELATION OF η FOR OPTIMUM DAMPING WITH THE SHOCK STRENGTH ξ'

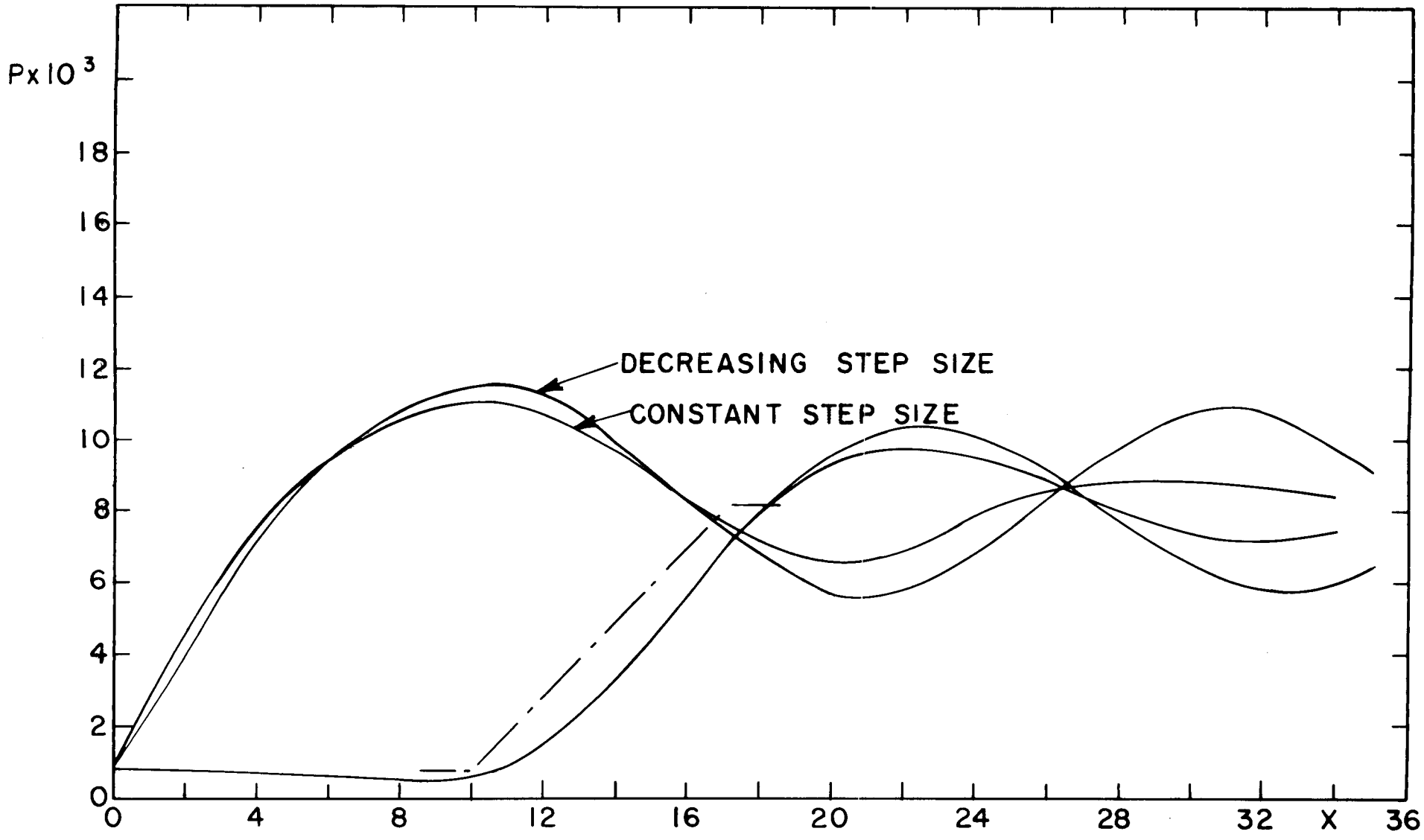

FIG. 10 : INFLUENCE OF ARTIFICIALLY DECREASED STEP SIZE ΔX.
$M_1 = 5$, $\delta = 30°$, $\gamma = 1.2$

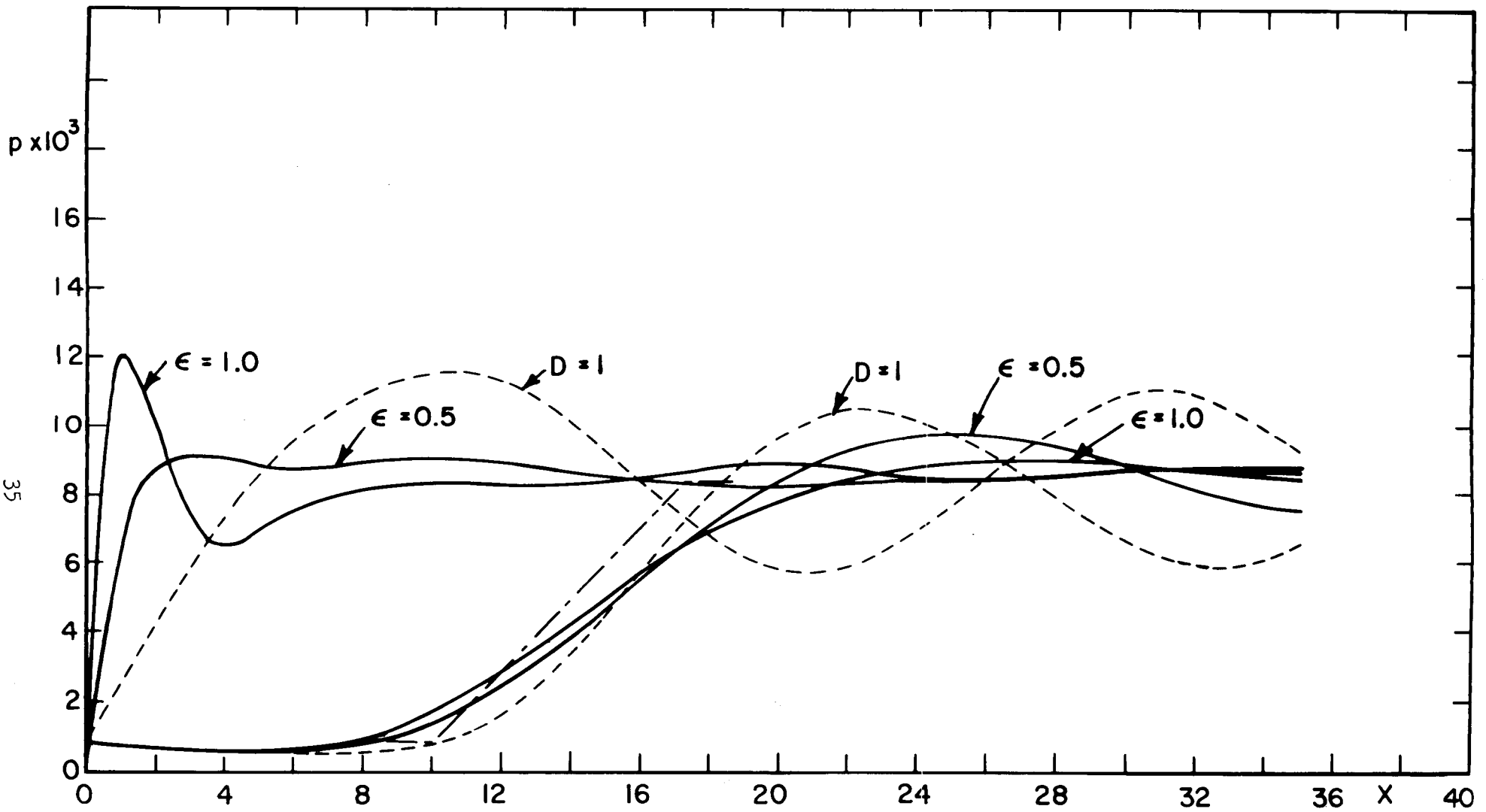

FIG. 11 : EXPERIMENT WITH THE METHOD OF LOCAL DAMPING AND ARTIFICIALLY DECREASING STEP SIZE ΔX. $M_1 = 5$, $\delta = 30°$, $\gamma = 1.2$

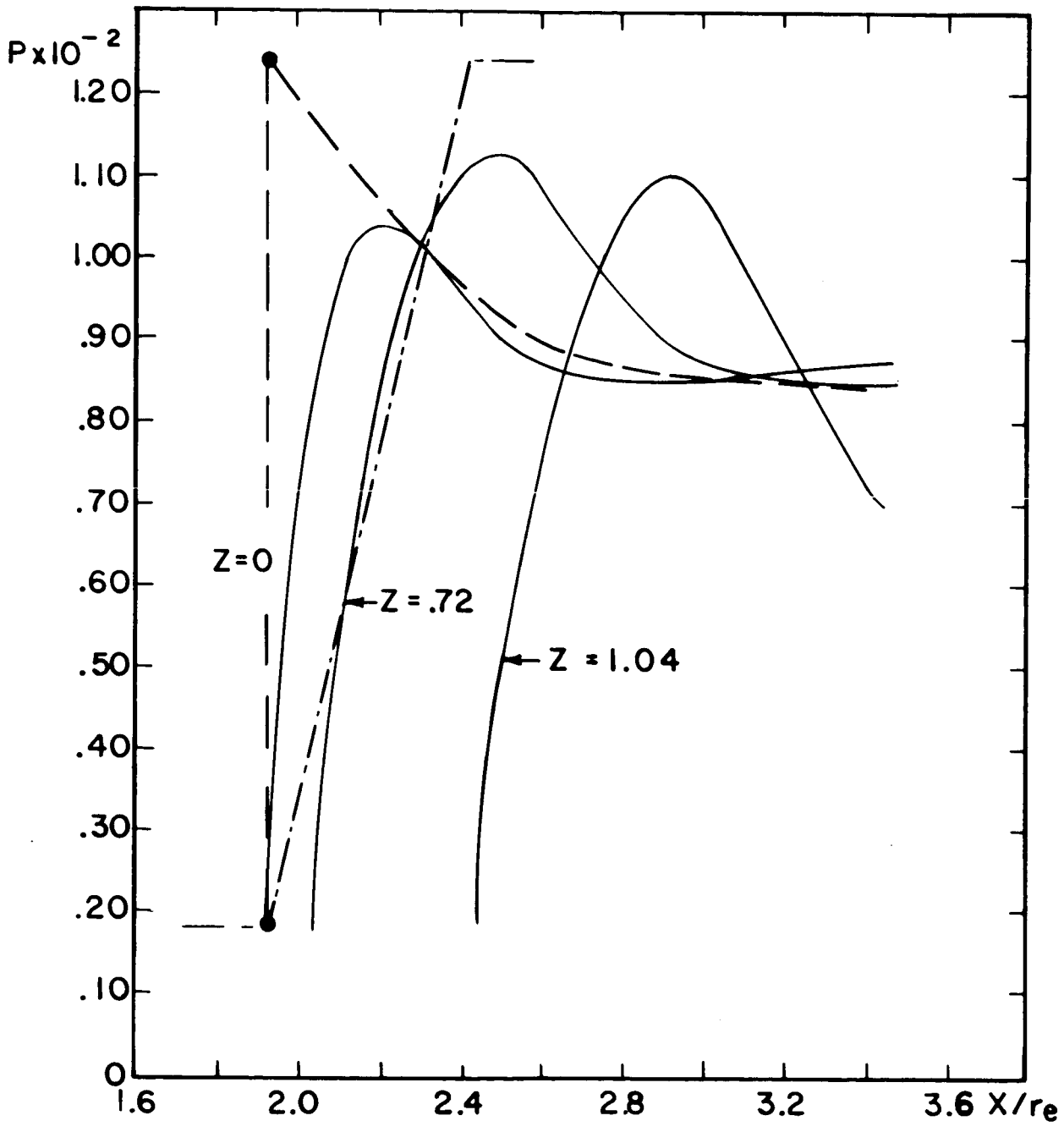

FIG. 12 : PRESSURE DISTRIBUTIONS IN THE PLANE AT INTERACTION

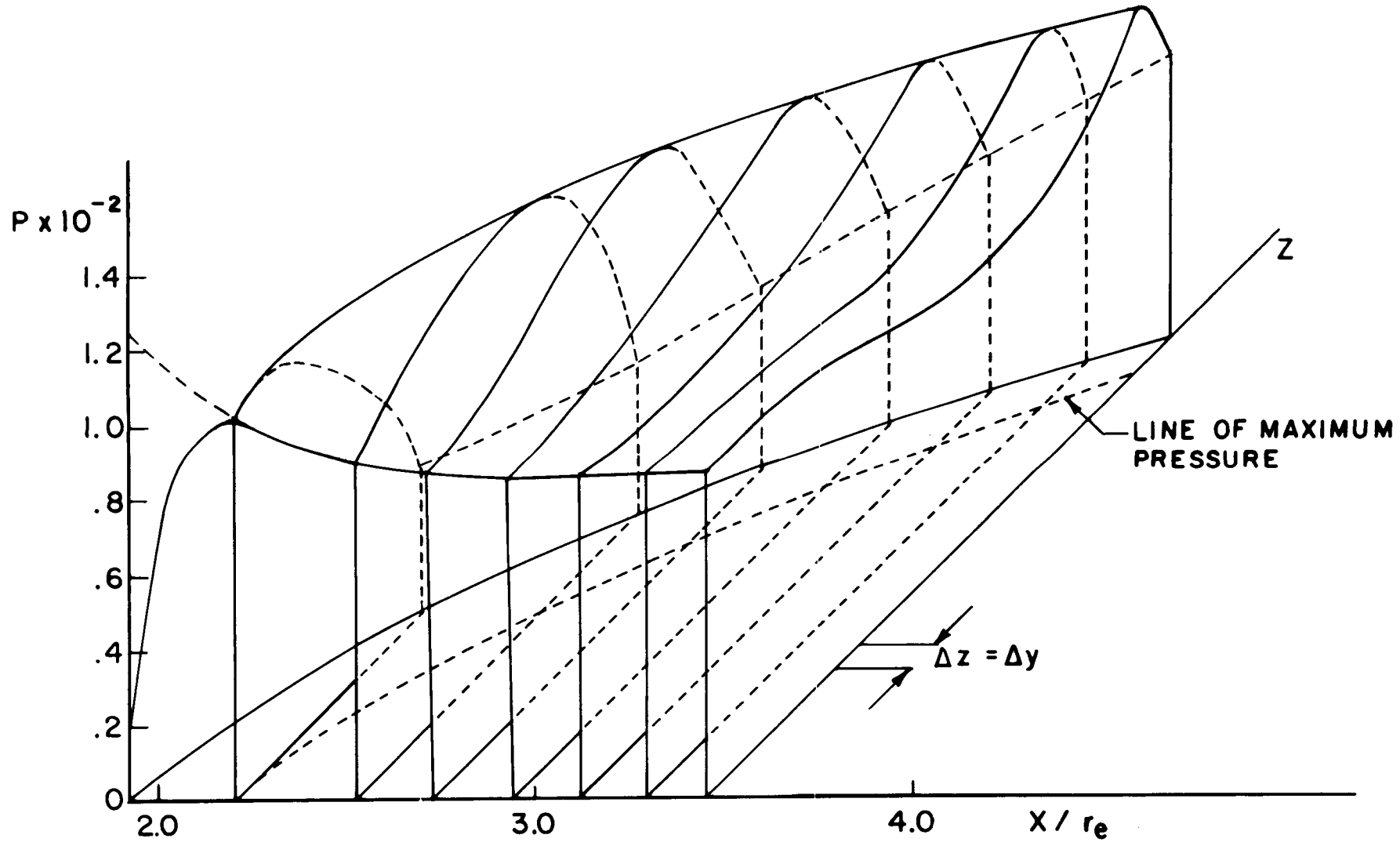

FIG. 13 : RELIEF OF THE PRESSURE DISTRIBUTION IN THE INTERACTION PLANE